RSC Advances

RSC Publishing

PAPER

View Article Online
View Journal | View Issue

Rheological model predicting compressive responses of carbon nanotube networks

Cite this: *RSC Advances*, 2013, **3**, 14473

Xinwei Tang,[a] Xuchun Gui,[b] Yulan Liu*[a] and Biao Wang[b]

Carbon nanotube (CNT) macrostructures like anisotropic CNT arrays and isotropic CNT networks have many unique mechanical properties. Among the various properties of CNT networks, their collective responses to compressive deformation are studied here. A rheological model is found to account for the mechanical properties of CNT networks. The computational results show that the compressive responses of CNT networks include the mechanical action of interconnected springs and dry friction elements. The availability of the model is validated by comparing the computed results to the measured data of different density CNT sponges. The good agreement between the computed and measured results suggests that the compressive responses of CNT segments and the sliding friction between CNTs are the major factors contributing to the compressive responses of CNT networks. The effectiveness of the model in describing the CNT networks also indicates that their collective responses are similar to that of the rheological model during the compression cycle.

Received 7th March 2013,
Accepted 20th May 2013

DOI: 10.1039/c3ra41108g

www.rsc.org/advances

Introduction

Carbon nanotube (CNT) macrostructures have been reported as possessing many unique mechanical properties. Examples are anisotropic vertically aligned CNTs with a high recovery rate and fatigue resistance under cyclic compression,[1] 2D isotropic buckydisks and buckypaper with a tunable in-plane Poisson's ratio,[2,3] 3D CNT networks like assembled traversing long CNTs with temperature-invariant viscoelasticity and isotropic CNT sponges with super compressibility.[4,5] Although the collective mechanical behavior of anisotropic CNT macrostructures like CNT arrays,[6] bundles,[7] and turfs have been studied intensely,[8] a thorough understanding of the collective response to compressive deformation of isotropic CNT networks and the major factors governing the response are still required.

The mechanical responses of CNT networks are, in nature, the response of individual CNTs in the network, which mainly stem from the properties of the CNTs and interactions between them.[2,4,9–13] Based on the stretching, bending, torsion and weak van der Waals (VDW) interactions of CNTs, simulations *via* coarse-grained molecular dynamics have been performed to explore the mechanical responses of CNT networks and the effect of nanosprings on the viscoelasticity of elastomeric polymers.[7,14,15] Yet, limited by the space size and timescale, it is difficult for molecular dynamics simulations to conduct enough experimental observations in the tiny scale to support the simulations. A model that considers the microstructures of CNT networks, the number of contacts between the CNTs and average distance between the contacts attempts to predict the compression resistances of buckydisks, however, the computed results overestimate the experimental data.[16]

In this work we use a rheological model to explore the compressive responses of 3D isotropic CNT networks. The rheological model mainly accounts for the bending behavior of CNT segments and sliding friction between CNTs. The compressive responses of CNT sponges are computed by the model and then compared to the measured data of CNT sponges, which share many similarities with other CNT networks like the randomly oriented microstructures and stress-strain hysteresis during compression cycles.

Experimental

As our previous work has shown, CNT sponges were synthesized by CVD methods, in which ferrocene and 1,2-dichlorobenzene were used as the catalyst precursor and carbon source, respectively.[5] The bulk density of the sponge can be tuned from about 5 to 100 mg cm^{-3} by changing the synthesis conditions. The microstructure and morphology of CNT sponges were characterized by scanning electron microscopy (SEM, S-4800). Prior to the mechanical tests, as-grown CNT sponges were peeled off from growth substrates and cut into cubic bulks with sizes of about $10 \times 10 \times 10$ mm^3. The tests were carried out by Instron 5843 equipped with 10 N/1 kN load cells and two flat-surface compression stages. The sample

[a]*School of Engineering, Sun Yat-Sen University, Guangzhou 510275, PR China. E-mail: stslyl@mail.sysu.edu.cn*
[b]*State Key Lab of Optoelectronic Materials and Technologies, School of Physics and Engineering, Sun Yat-Sen University, Guangzhou 510275, PR China*

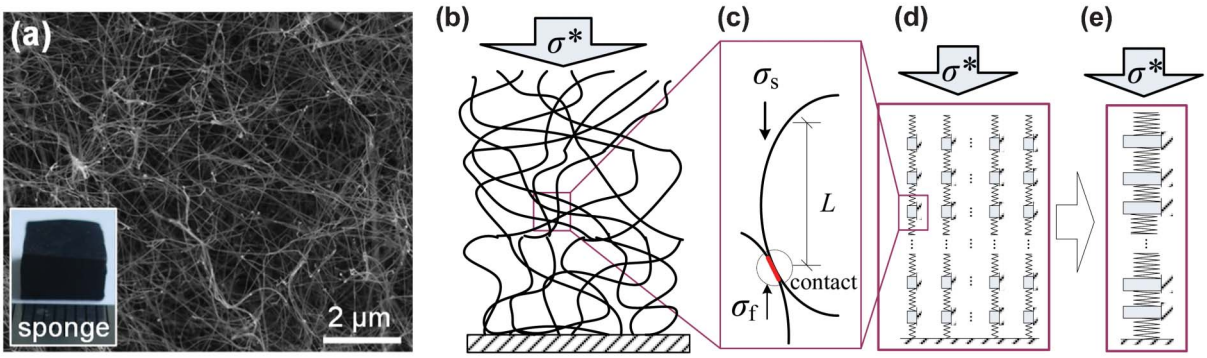

Fig. 1 (a) The SEM image of a CNT network showing that intertwining CNTs form a porous network; inset, photo of an as-grown CNT network. (b) Schematic of the CNT network with a 3D random structure under compression. (c) Schematic of a CNT segment in the network subject to compression from other CNTs (σ_s) and sliding friction at the node where CNTs contact (σ_f). (d) The model for the entire CNT network containing the micro-springs and dry friction elements in series and parallel. (e) The rheological model with the converged macro-springs and dry friction elements.

was uniaxially compressed along the height (or its growth direction) and the compressive rate was set in the range of 4 mm min^{-1}.

Results and discussion

The SEM image (Fig. 1a) shows that an as-grown CNT sponge consists of curving CNTs, which randomly intertwine and form a porous 3D network. Each CNT overlaps with other CNTs at different positions, resulting in numerous contacts of CNTs within the network. TEM images show that these CNTs are MWCNT (multi-walled nanotubes) with diameters from 30 to 50 nm. For a porous CNT sponge under compression, it is CNTs that actually bear the external load (Fig. 1b). Previous experiment has shown that the mechanical strength of a CNT sponge is highly affected by its porosity.[17] Based on the SEM observations, a full-length CNT can be divided into many segments at the positions where the CNT contacts with other CNTs. The length of the segment between contacts (L) can be directly observed in SEM images (Fig. 1a). The segment is subject to compression from other CNTs and a sliding friction between CNTs (Fig. 1c).[10] Since the stress-strain curve of a CNT network during the compression cycle is always accompanied with an obvious hysteresis loop, which indicates energy dissipation and friction within the network,[17] we think that the sliding friction between CNTs in contact derived from VDW forces is insufficient to resist their relative sliding during compression. Thus, this sliding friction stress between CNTs is represented by a dry friction element with the critical stress σ_f.

A micro-spring with the length L is used to represent the CNT segment whose stiffness is measured by the compressive response of the bent segment (E_s). For the whole CNT network, this can be represented by identical segments that are connected in series and parallel (Fig. 1d). The parallel segments at the same height, representing one layer of the CNT network, can be combined into a macro-spring due to the uniaxial compression. The stiffness of the macro-springs is denoted by E^*. Correspondingly, the sliding frictions between CNTs are also converged into a friction of σ_f^* between the layers.

Since it is the individual CNTs that actually bear the external compression to the porous CNT network, the relations between the two sorts of springs and dry friction elements are converted through the fraction volume occupied by CNTs:

$$E^* = \varphi_0 E_s \qquad \sigma_f^* = \varphi_0 \sigma_f \tag{1}$$

where φ_0 is the initial fraction volume of the sponge. This leads to a rheological model of interconnected springs and dry friction elements (Fig. 1e). A similar triboelastic model was also used to study the stress-strain hysteresis of CNT macrostructures.[14]

The stiffness of a single CNT segment (Fig. 1c) is obtained by calculating the compressive modulus of the bent segment (E_s) (Fig. 2). Considering a CNT segment with an initially curved shape, a vertical compressive stress (σ_s) is applied at its contacts with other CNTs. The strain of the segment (ε) is

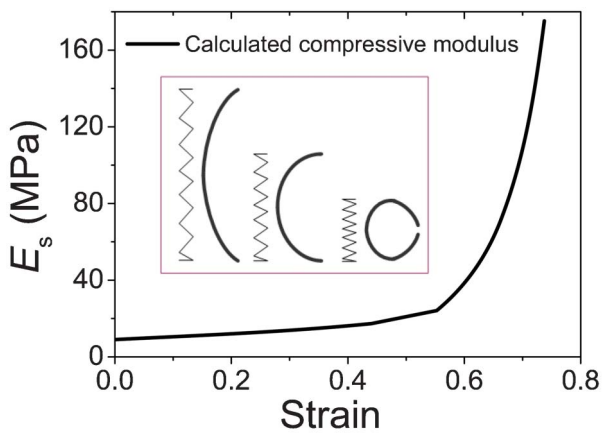

Fig. 2 Modeling of a CNT segment under compression using Euler beam theory. (a) The calculated compressive modulus-strain curve of the CNT segment. Inset, illustrated deformation process of a CNT segment under compression.

defined as the normalized variance of the height of the CNT segment (L). The CNT segment can be considered as an elastic beam, due to the inherent capacity of CNTs to fully recover under large strain and repeated bending,[9,12] and Euler beam theory is adopted to analyze the compressive response.[8,11,13,18–21] Parameters of the elastic beam are given on the basis of SEM and TEM observations of CNT segments, with outer diameters of about 40 nm and heights of about 5 μm. Given the approximate Young's modulus of CNTs ($\sim$1 TPa),[22] the compressive stress-strain response of the beam can be analyzed and the compressive modulus (E_s) is calculated by taking the differentiation of the stress with respect to the strain of the beam (Fig. 2).

The critical stress (σ_f) of the sliding friction can be calculated according to the frictional force between CNTs (f) and the cross-sectional area (A_s) of a CNT in the network. *In situ* mechanical experiments showed that the frictional force between CNTs and the defects present on the CNTs only causes some slight fluctuations during the measurement.[10] Since CNTs only contact with each other at the outmost wall, the difference in CNT diameter between our experiment and the *in-situ* mechanical experiment can be neglected and the frictional force (f) from literature data is directly adopted (4 pN). Then, the frictional stress (σ_f) is obtained by:

$$\sigma_f = \frac{f}{A_s} \tag{2}$$

where A_s is the average cross-sectional area of the CNTs (40 nm obtained from TEM images).

The stress-strain response of the rheological model is determined by the collective responses of the springs and dry friction elements during the compression cycle (Fig. 3). In the model, an engineering compressive stress (σ^*) is applied on the topmost macro-spring and the downmost spring is fixed, corresponding to the CNT network compressed between two flat stages. During loading, in the first stage the macro-springs are activated in sequence from top to bottom and the corresponding stress-strain response of the model is a piece-wise curve with many line segments. After the last spring at the bottom is activated, all the springs are involved in the compressing process so that the stress-strain curve in this stage becomes straight. During unloading, the directions of all the frictional stresses reverse, which leads to a similar activating process from top to bottom, yet with the activating period doubled. The difference in the activating periods during loading and unloading causes the springs near the bottom to be unable to recover fully. This means that after the loading is removed a residual strain of the model is left, which agrees with the experimental observations.

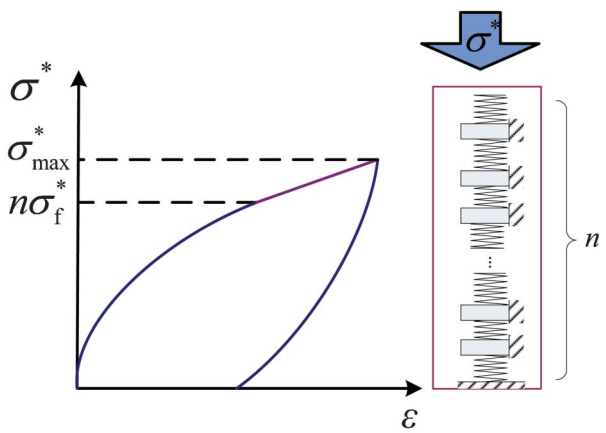

Fig. 3 The stress-strain response of the rheological model for the entire CNT network. Inset, illustration of the model with n + 1 springs and n dry friction elements.

The detailed stress-strain response of the rheological model for the compression cycle is analyzed as follows. The strain of the model (ε^*) is defined as the normalized compressed displacement of the free end. For the entire CNT sponge with n layers along its height, n + 1 springs and n dry friction elements are set in the model.

For the piece-wise response of the model with many line segments, let (ε_i^*, σ_i^*) be the coordinates of the end point of the i-th segment. According to the series connection of the springs, the global stiffness of the model during the i-th segment (E_i) is

$$E_i = \frac{n}{i} E^* \tag{3}$$

The stress period of the i-th segment ($\Delta\sigma^*$) simply equals to one frictional stress σ_f^*. The strain period of the i-th segment is obtained by dividing the stress period ($\Delta\sigma^*$) by the global stiffness of the model (E_i):

$$\Delta\varepsilon_i^* = \frac{\Delta\sigma^*}{E_i} = \frac{\sigma_f^*}{\frac{n}{i}E^*} \tag{4}$$

By superimposing the strain period $\Delta\varepsilon_i^*$, the coordinates of the end point of the i-th linear segment (ε_i^*, σ_i^*) can be obtained:

$$\varepsilon_i^* = \sum_{k=1}^{i} \Delta\varepsilon_k^* = \frac{1}{2} i(i+1) \frac{\sigma_f^*}{nE^*} \tag{5}$$

with the stress value of the end point summed by i dry frictional stresses:

$$\sigma_i^* = i\sigma_f^* \tag{6}$$

Combining eqn (5) and (6), the stress-strain response of the model at the first stage during loading can be obtained

$$\varepsilon_i^* = \frac{\sigma_i^* \left(\frac{\sigma_i^*}{\sigma_f^*} + 1 \right)}{2nE^*} \tag{7}$$

Since the number of the springs (n) is more than one thousand (computed by dividing the thickness of the sponge H

by the distance between contacts (L)), the limiting case for eqn (7) is shown in eqn (8):

$$\varepsilon_i^* \approx \frac{(\sigma_i^*)^2}{2n\sigma_f^* E^*} \quad (n \to \infty) \tag{8}$$

This turns out to be a smooth curve instead of a piece-wise one with many line segments. The linear segment becomes very short in the limiting case so that the discrete end points (ε_i^*, σ_i^*) can be viewed as continuous ones (ε^*, σ^*) along the smooth curve. So, the stress-strain relation eqn (8) is rewritten as:

$$\sigma^* = \sqrt{2F^* E^* \varepsilon^*} \quad (0 \le \sigma^* \le F^*) \tag{9}$$

where F^* is the resultant of the sliding frictional stress of all layers:

$$F^* = n\sigma_f^* \tag{10}$$

When the external stress σ^* exceeds the upper limit in the first stage (F^*), all the springs are activated and the stress-strain response of the rheological model turns to be linear:

$$\sigma^* = E^* \varepsilon^* \ (F^* < \sigma^* \leqslant \sigma_{max}^*) \tag{11}$$

During unloading, the stress-strain response is a reversed version of the process during loading, with the curve beginning at (ε_{max}^*, σ_{max}^*) and the period doubled:

$$\sigma_{max}^* - \sigma^* = \sqrt{4F^* E^* (\varepsilon_{max}^* - \varepsilon^*)} \quad ((\sigma_{max}^* - 2F^*) < \sigma^* \le \sigma_{max}^*) \tag{12}$$

Eqn (9) and (12) are differentiated first and then computed by numerical integration with the stiffness $E^*(\varepsilon)$ discretized in the computation, considering the increase of E^* with the strain (Fig. 2b).

$$\sigma_{k+1}^* = \begin{cases} \sigma_k^* + \sqrt{\dfrac{F^* E^* (\varepsilon_{k+1}^*)}{2\varepsilon_{k+1}^*}} \Delta\varepsilon^* & (0 \le \sigma_k^* \le F^*) \\ \sigma_k^* + E^* (\varepsilon_{k+1}^*) \Delta\varepsilon^* & (F^* < \sigma_k^* \le \sigma_{max}^*) \end{cases} \tag{13}$$

The strain integration step in the computation ($\Delta\varepsilon^*$) is the same and the initial condition for the loading is:

$$\sigma_1^* = \varepsilon_1^* = 0 \tag{14}$$

The response during unloading is computed by:

$$\sigma_{k+1}^* = \begin{cases} \sigma_k^* - \sqrt{\dfrac{F^* E^* (\varepsilon_{k+1}^*)}{\varepsilon_{max}^* - \varepsilon_{k+1}^*}} \Delta\varepsilon^* & ((\sigma_{max}^* - 2F^*) < \sigma_k^* \le \sigma_{max}^*) \\ \sigma_k^* - E^* (\varepsilon_{k+1}^*) \Delta\varepsilon^* & (0 \le \sigma_k^* \le (\sigma_{max}^* - 2F^*)) \end{cases} \tag{15}$$

with the initial conditions:

$$\sigma_1^* = \sigma_{max}^* \text{ and } \varepsilon_1^* = \varepsilon_{max}^* \tag{16}$$

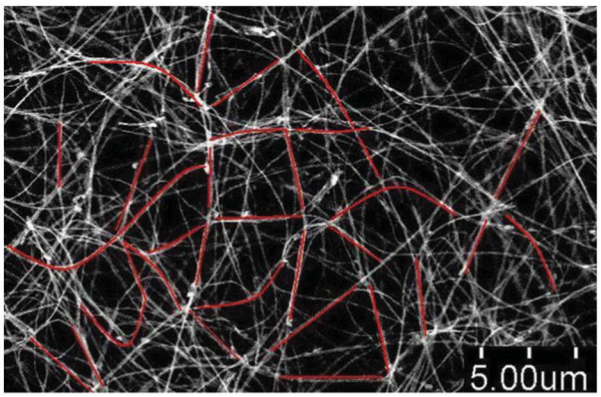

Fig. 4 SEM image of the CNT sponge showing CNT segments joining two contacts (marked in red). The average value of the distance between contacts joined by a CNT segment is obtained by manually picking the contacts and calculating the average value.

Now the compressive responses of CNT networks can be numerically computed with the following parameters. The initial fraction volume of the CNT network (φ_0) in eqn (1) is obtained by dividing the bulk density (ρ^*) of the CNT network by the density of CNTs (2.1 g cm^{-3}). The length of a CNT segment joining two contacts (L) is obtained by first identifying CNT segments joining two contacts in the SEM images (CNT segments marked as red in Fig. 4). The lengths of these CNT segments and their average value are calculated according to the SEM observation (calculated results show that the average value changes from 3 to 9 μm depending on the CNT sponge's bulk density). Then, the stiffness (E_s) of the micro-springs can be computed using Euler beam theory as mentioned before (Fig. 2). The sliding friction between CNTs (σ_f) is calculated by eqn (2). Then, the stiffness (E_s) and the sliding friction stress (σ_f) are converted to the E^* and F^* values according to eqn (1) and (10). The compressive modulus- and stress-strain relations of the model are computed by eqn (13) and (15), with the results shown in Fig. 5.

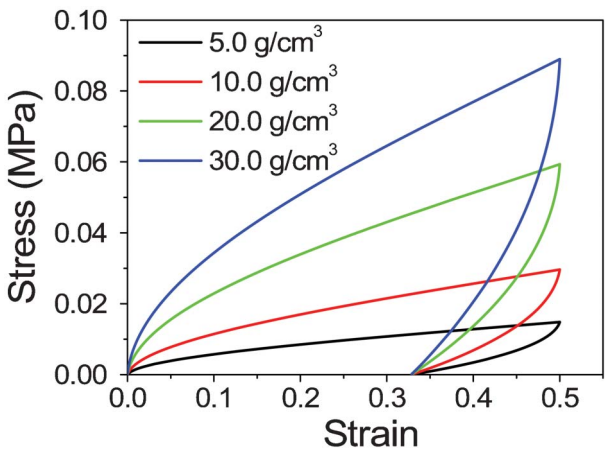

Fig. 5 Computed compressive stress- and modulus-strain responses of CNT networks with different densities by the rheological model.

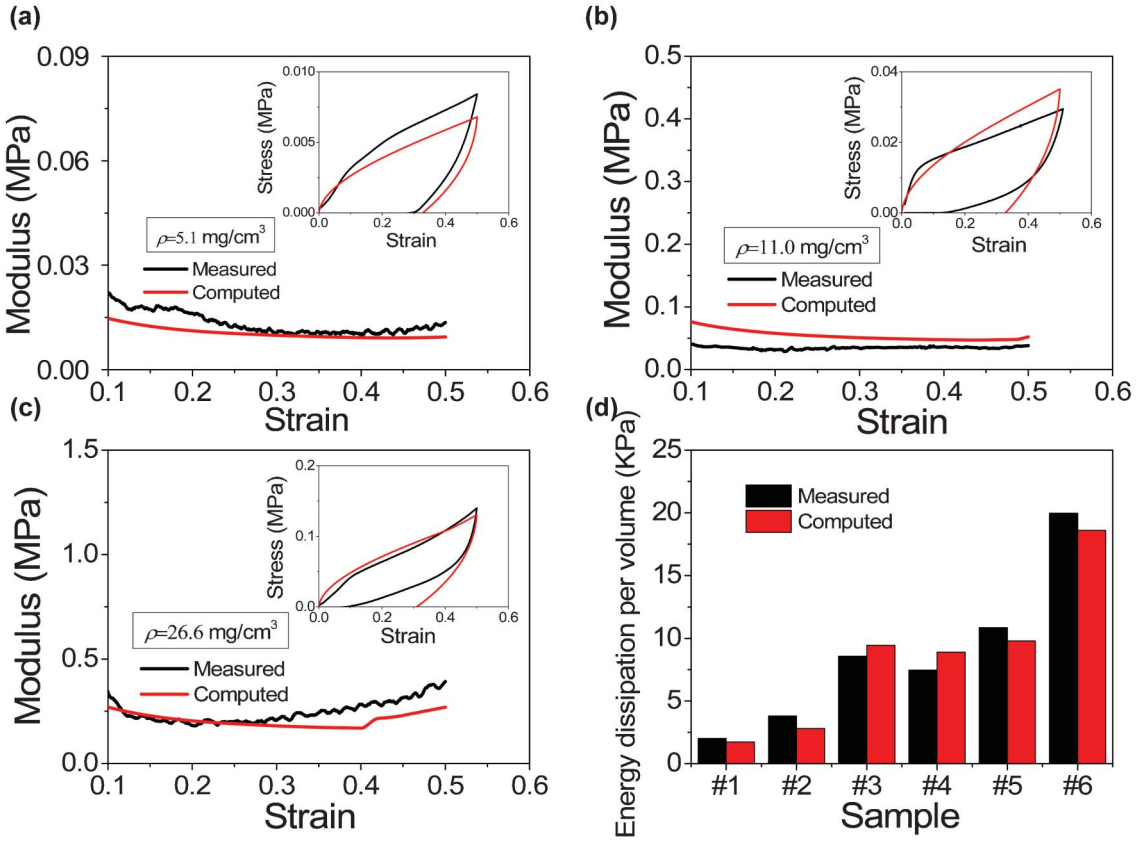

Fig. 6 Validation of the rheological model by computing the compressive modulus-strain curves during loading and stress-strain curves during the compression cycle and comparing them to the measured ones, choosing samples with the densities of (a) 5.1 mg cm^{-3} (b) 11.0 mg cm^{-3} and (c) 26.6 mg cm^{-3}. (d) The computed and measured energy dissipation for more samples under different testing conditions.

CNT sponges with different densities are chosen as samples and their compressive responses are measured by the rheological model. Direct comparisons between the computed results from the rheological model and the measured data are shown in Fig. 6. For the CNT sponge with a density of 5.1 mg cm^{-3}, the compressive response computed by the model is a little lower than the measured one. The computed compressive modulus during loading is ~0.015 MPa compared to the measured ~0.02 MPa and the computed maximum stress is ~0.006 MPa compared to the measured ~0.008 MPa (Fig. 6a). For the 11.0 mg cm^{-3} sample, the computed result overestimates the compressive modulus during loading (computed ~0.07 MPa compared to measured ~0.05 MPa) (Fig. 6b). The comparison for the 26.6 mg cm^{-3} sample is shown in Fig. 6c, with a general agreement between computation and measurement. The main difference still occurs during unloading (computed ~30% residual strain compared to ~10% measured). For more samples with different densities, the measured and computed energy dissipations per volume during the compression cycle were computed and the comparison is shown in Fig. 6d and Table 1. It can be seen from the comparisons that the computed results by the model are close to the measured ones, which proves that the rheological model has successfully captured the major mechanism of the CNT networks' responses under compression.

Table 1 Comparison of the energy dissipation per volume for different samples

Sample Unit	Bulk density of CNT sponge (mg cm^{-3})	Maximum strain	Measured energy dissipation per volume (KPa)	Computed energy dissipation per volume (KPa)
#1	5.1	0.5	2.01	1.72
#2	5.8	0.6	3.80	2.80
#3	7.3	0.6	8.56	9.43
#4	11.0	0.5	7.45	8.89
#5	12.1	0.5	10.85	9.78
#6	12.1	0.7	19.97	18.60

The difference between the measured and computed curves mainly appears during unloading. The difference may come from the residual strain, whose mechanism has not been fully understood. Previous experiments have shown that CNT sponges immersed in organic solvents can recover to almost their original shape even under cyclic compression, while in air a residual strain will be observed. Moreover, the residual strain during cyclic compression always changes in every cycle.[5] Thus, there should be a more complex mechanism governing the residual strain. Other minor factors for the observed difference may include the friction between CNTs, whose value is adopted from literature data,[10] while in our case the frictional force may be slightly different. The contribution of defects and catalysts embedded in CNTs are also considered to be minor since they occupy only a very small proportion in CNTs.

The interactions between CNTs were attributed to the adhesion during the detachment of CNT contacts and sliding friction at CNT contacts. Although both of the interactions stem from the large VDW attraction between CNTs,[6] the sliding friction was calculated to be $\sim$4 pN and the adhesion was calculated to have a much larger value of about 0.7 nN.[10] During the computation of the compressive responses of CNT networks, the results obtained by applying the value of the sliding friction fit much better with the measured ones than applying the value of adhesion, which suggests that the interactions between CNTs during the compression of CNT networks are mainly in the form of sliding friction. This process is distinct from that of CNT network shearing tests, in which the interaction was assumed as reversible detachment and attachment between CNTs.[4]

Motivated by the rheological model, the collective response of CNT networks during the compression cycle can also be described as follows. In the initial stage during loading, the CNTs near the top layer are compressed first and the CNTs intertwining underneath are blocked by the friction between CNTs. As the loading continues, the sliding friction is overcome so that all the CNTs are involved in the compression. During unloading, the direction of each sliding friction reverses so that the CNTs still need to overcome the resistance coming from the friction before they are able to recover. The longer period during unloading for the CNTs to overcome the friction can also explain the residual strain observed in the compressive tests.

Conclusions

In this article we studied the collective responses of CNT networks to compressive deformation by founding a rheological model. The model mainly accounts for the mechanical properties of CNTs and the sliding friction between CNTs, which are represented by springs and dry friction elements, respectively. With the parameters based on experimental observations and the literature, the compressive responses of CNT networks under different testing conditions were computed by the model and then compared to the measured data. The good agreement between the computed and measured results suggests that the compressive responses of CNT segments and the sliding friction between CNTs are the major factors contributing to the compressive responses of CNT networks. The effectiveness of the model in describing the CNT networks also indicates that their collective responses are similar to that of the rheological model during the compression cycle.

Since the SEM observations show that CNT sponges share many similarities in their microstructures with other CNT networks like buckypaper, buckydisks and assembled traversing long CNTs, the rheological model for CNT sponges may also be applicable to other CNT networks, which may be one of the future directions of the present work. Other directions might include predicting the mechanical responses of CNT sponges more accurately by calculating the distance between contacts with an image analysis procedure.

Acknowledgements

This work is supported by National Natural Science Foundation of China (Grant No. 11072271, 11232015, 10972239 and 51102286) and Specialized Research Fund for the Doctoral Program of Higher Education (No. 20120171110005).

Notes and references

1 A. Y. Cao, P. L. Dickrell, W. G. Sawyer, M. N. Ghasemi-Nejhad and P. M. Ajayan, Super-compressible foamlike carbon nanotube films, *Science*, 2005, **310**, 1307–10.
2 R. L. D. Whitby, T. Fukuda, T. Maekawa, S. L. James and S. V. Mikhalovsky, Geometric control and tuneable pore size distribution of buckypaper and buckydiscs, *Carbon*, 2008, **46**, 949–56.
3 L. J. Hall, V. R. Coluci, D. S. Galvao, M. E. Kozlov, M. Zhang, S. O. Dantas and R. H. Baughman, Sign change of Poisson's ratio for carbon nanotube sheets, *Science*, 2008, **320**, 504–7.
4 X. Ming, D. N. Futaba, T. Yamada, M. Yumura and K. Hata, Carbon nanotubes with temperature-invariant viscoelasticity from 196° to 1000 °C, *Science*, 2010, **330**, 1364–8.
5 X. Gui, J. Wei, K. Wang, A. Cao, H. Zhu, Y. Jia, Q. Shu and D. Wu, Carbon nanotube sponges, *Adv. Mater.*, 2010, **22**, 617–621.
6 L. Qu, L. Dai, M. Stone, Z. Xia and Z. L. Wang, Carbon nanotube arrays with strong shear binding-on and easy normal lifting-off, *Science*, 2008, **322**, 238–42.
7 S. B. Hutchens, L. J. Hall and J. R. Greer, *In situ* Mechanical testing reveals periodic buckle nucleation and propagation in carbon nanotube bundles, *Adv. Funct. Mater.*, 2010, **20**, 2338–46.
8 A. A. Zbib, S. D. Mesarovic, E. T. Lilleodden, D. McClain, J. Jiao and D. F. Bahr, The coordinated buckling of carbon nanotube turfs under uniform compression, *Nanotechnology*, 2008, **19**, 175704.
9 M. R. Falvo, G. J. Clary, R. M. Taylor, V. Chi, F. P. Brooks, S. Washburn and R. Superfine, Bending and buckling of

carbon nanotubes under large strain, *Nature*, 1997, **389**, 582–4.
10 B. Bhushan, X. Ling, A. Jungen and C. Hierold, Adhesion and friction of a multiwalled carbon nanotube sliding against single-walled carbon nanotube, *Phys. Rev. B: Condens. Matter Mater. Phys.*, 2008, **77**.
11 H. W. Yap, R. S. Lakes and R. W. Carpick, Mechanical instabilities of individual multiwalled carbon nanotubes under cyclic axial compression, *Nano Lett.*, 2007, **7**, 1149–54.
12 S. Iijima, C. Brabec, A. Maiti and J. Bernholc, Structural flexibility of carbon nanotubes, *J. Chem. Phys.*, 1996, **104**, 2089–92.
13 T. Kuzumaki and Y. Mitsuda, Nanoscale mechanics of carbon nanotube evaluated by nanoprobe manipulation in transmission electron microscope, *Jpn. J. Appl. Phys.*, 2006, **45**, 364–8.
14 X. Yang, P. He and H. Gao, Modeling frequency and temperature-invariant dissipative behaviors of randomly entangled carbon nanotube networks under cyclic loading, *Nano Res.*, 2011, **4**, 1191–8.
15 J. Liu, Y.-L. Lu, M. Tian, F. Li, J. Shen, Y. Gao and L. Zhang, The interesting influence of nanosprings on the viscoelasticity of elastomeric polymer materials: simulation and experiment, *Adv. Funct. Mater.*, 2013, **23**, 1156–63.
16 S. V. Lomov, L. Gorbatikh and I. Verpoest, A model for the compression of a random assembly of carbon nanotubes, *Carbon*, 2011, **49**, 2079–91.
17 X. Gui, A. Cao, J. Wei, H. Li, Y. Jia, Z. Li, L. Fan, K. Wang, H. Zhu and D. Wu, Soft, highly conductive nanotube sponges and composites with controlled compressibility, *ACS Nano*, 2010, **4**, 2320–6.
18 R. M. Jones, *Buckling of Bars, Plates, and Shells*, Bull Ridge Publishing, 2006.
19 T. Tong, Y. Zhao, L. Delzeit, A. Kashani, M. Meyyappan and A. Majumdar, Height independent compressive modulus of vertically aligned carbon nanotube arrays, *Nano Lett.*, 2008, **8**, 511–5.
20 J. F. Waters, L. Riester, M. Jouzi, P. R. Guduru and J. M. Xu, Buckling instabilities in multiwalled carbon nanotubes under uniaxial compression, *Appl. Phys. Lett.*, 2004, **85**, 1787–9.
21 B. I. Yakobson, C. J. Brabec and J. Bernholc, Nanomechanics of carbon tubes: instabilities beyond linear response, *Phys. Rev. Lett.*, 1996, **76**, 2511–4.
22 T. Fukuda, F. Arai and L. Dong, Assembly of nanodevices with carbon nanotubes through nanorobotic manipulations, *Proc. IEEE*, 2003, **9**, 1803–18.